

An automated nudged elastic band method

Esben L. Kolsbjerg, Michael N. Groves, and Bjørk Hammer

Citation: [The Journal of Chemical Physics](#) **145**, 094107 (2016); doi: 10.1063/1.4961868

View online: <http://dx.doi.org/10.1063/1.4961868>

View Table of Contents: <http://aip.scitation.org/toc/jcp/145/9>

Published by the [American Institute of Physics](#)

Articles you may be interested in

[A climbing image nudged elastic band method for finding saddle points and minimum energy paths](#)
The Journal of Chemical Physics **113**, 9901 (2000); 10.1063/1.1329672

[Energy landscapes and persistent minima](#)

The Journal of Chemical Physics **144**, 054109 (2016); 10.1063/1.4941052

[Communication: Constant uncertainty molecular dynamics: A simple and efficient algorithm to incorporate quantum nature into a real-time molecular dynamics simulation](#)

The Journal of Chemical Physics **145**, 171101 (2016); 10.1063/1.4966917

[Improved tangent estimate in the nudged elastic band method for finding minimum energy paths and saddle points](#)

The Journal of Chemical Physics **113**, 9978 (2000); 10.1063/1.1323224

[Global and local curvature in density functional theory](#)

The Journal of Chemical Physics **145**, 054109 (2016); 10.1063/1.4959882

[Communication: Inverse design for self-assembly via on-the-fly optimization](#)

The Journal of Chemical Physics **145**, 111101 (2016); 10.1063/1.4962754

**COMPLETELY
REDESIGNED!**

**PHYSICS
TODAY**

Physics Today Buyer's Guide
Search with a purpose.

An automated nudged elastic band method

Esben L. Kolsbjerg, Michael N. Groves, and Bjørk Hammer^{a)}

Interdisciplinary Nanoscience Center (iNANO), Department of Physics and Astronomy, Aarhus University, Aarhus C, Denmark

(Received 15 June 2016; accepted 9 August 2016; published online 2 September 2016)

A robust, efficient, dynamic, and automated nudged elastic band (AutoNEB) algorithm to effectively locate transition states is presented. The strength of the algorithm is its ability to use fewer resources than the nudged elastic band (NEB) method by focusing first on converging a rough path before improving upon the resolution around the transition state. To demonstrate its efficiency, it has been benchmarked using a simple diffusion problem and a dehydrogenation reaction. In both cases, the total number of force evaluations used by the AutoNEB method is significantly less than the NEB method. Furthermore, it is shown that for a fast and robust relaxation to the transition state, a climbing image elastic band method where the full spring force, rather than only the component parallel to the local tangent to the path, is preferred especially for pathways through energy landscapes with multiple local minima. The resulting corner cutting does not affect the accuracy of the transition state as long as this is located with the climbing image method. Finally, a number of pitfalls often encountered while locating the true transition state of a reaction are discussed in terms of systematically exploring the multidimensional energy landscape of a given process. Published by AIP Publishing. [<http://dx.doi.org/10.1063/1.4961868>]

I. INTRODUCTION

A reoccurring task in the theoretical study of catalytic surfaces and reactions is that of locating transition states (TS) in diffusion^{1–6} and chemical reaction mechanisms.^{7–25} This is not always a trivial problem and many different approaches have been formulated including different chain-of-state methods like the nudged elastic band (NEB) method,²⁶ Lanczos type schemes²⁷ such as the activation-relaxation technique nouveau (ARTn),²⁸ and the dimer method.²⁹ One advantage of the dimer and the ARTn methods is that no final state is necessary when searching for the transition state. They work by following the energy landscape uphill to the saddle point. The difference being that the dimer method uses only the first order derivative of the potential energy, while the ARTn method follows the eigenvector to the Hessian corresponding to the largest negative eigenvalue.

When the final state of a chemical process is available, it is much easier and more effective to use the NEB method since there is no guarantee that a method exclusively relying on local information, like the ARTn and dimer methods, will locate a transition state that directly links the initial and final states. The NEB works by converging an initial “guessed” path to the minimum energy path (MEP) in the immediate vicinity of the initial path. The minimization of all the intermediate images brings the path to the MEP where an image is a snapshot of the geometry of the progressed reaction. The images are moved according to a linear restoring spring force based on the distance between neighboring images and the local tangent of the path as well as the forces from the energy landscape perpendicular to the local

tangent. The initial guess for the MEP is typically created by an interpolation of the atomic positions that is akin to a straight line connecting the initial and final images. In a very basic NEB, which we will refer to as an *all-image* NEB method, all the images are supplied at the beginning of a NEB calculation and are subsequently relaxed to the local MEP.

Regardless of Moore’s law, which predicts continued exponential growth of computational power, it is still very important to efficiently deploy currently available resources. This is achieved by analysing modern procedures to determine suitable improvements. For instance, the *all-image* NEB approach relaxes all intermediate images to the minimum energy path (MEP) closest to the initial guessed pathway. Depending on the initial guess, this could mean that the path must be displaced very far in space as displayed in the top row of Figure 1. If the objective is to locate the TS with the fewest possible resources, an improved strategy would be to start with fewer images to define the reaction path, then add images only around the apparent peak thereby reducing the overall number of relaxation steps and focusing resources on the important regions. This method is illustrated in the bottom row of Figure 1. This is one example of a range of different suggested improvements to a regular NEB.^{30–32}

Here we present an add-on for the NEB method which is based on the strategy proposed above and is available in the ASE³³ software package. The outline of the paper is as follows: first Sec. II contains the outline of the AutoNEB algorithm and the details of the computational setup. Next, we present the benchmarking results against an *all-image* NEB followed by a discussion of common pitfalls. Identifying problematic issues is especially relevant when developing an automated

^{a)}Electronic mail: hammer@phys.au.dk.

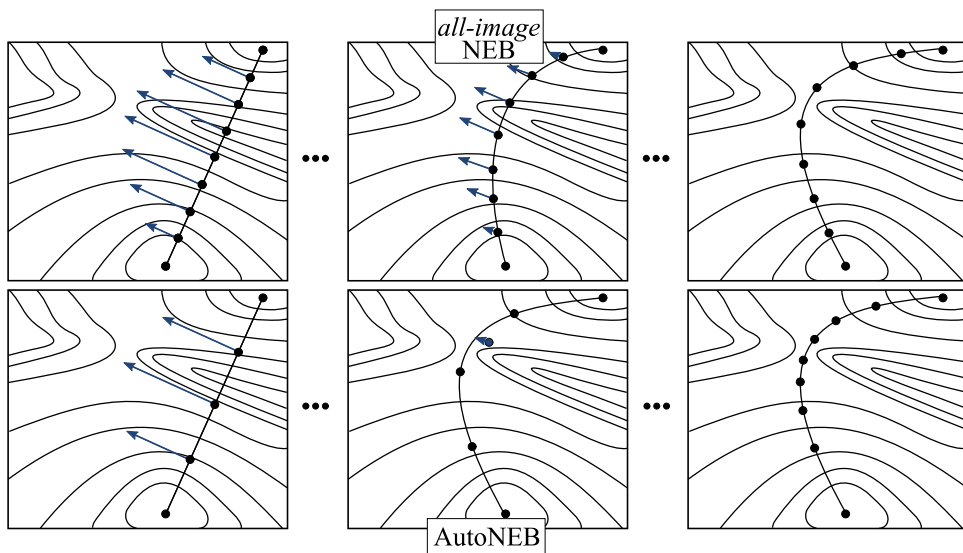


FIG. 1. Top row sketches snapshots of an *all-image* NEB strategy while the bottom row sketches snapshots of the AutoNEB strategy. In the latter, images are not added all at once, but instead dynamically so that new images are focused in the region of interest: the area around the peak.

implementation to locate TSs. We first deal with the possibility of finding the right saddle point in a complex energy landscape with multiple potential saddle points before finishing with an intrinsic instability of a regular NEB formulation that we have identified and discuss an alternative formulation where real springs are introduced.

II. METHOD

A. Algorithm

The AutoNEB algorithm employs the basic NEB method and acts as an add-on. The procedure is outlined in the flowchart in Figure 2. It has been clustered into two subgroups: an initialization phase and the main loop. An optional, final post-processing phase is described in the [supplementary material](#). While running an AutoNEB optimization the algorithm handles N images, where N is a growing number starting from the number of user-supplied images (at least two, the initial and final image). The strategy is to perform the NEB only on a subset size: N_{sim} , of the N images. The N_{sim} images are always picked as sequential images centred on any images newly added by the algorithm. The strategy is to evaluate pieces of the path step by step to converge a rough path before adding more images. The size of individual pieces is specified by the user as a chosen number of images, N_{sim} . Typically, one chooses to focus on the area around the peak adding images here to improve the estimate of the TS.

All that is required are the two end points for which a NEB path is requested; however, a flexible number of intermediate images can also be supplied as a user inputted guess of the MEP when the AutoNEB is initialized. The AutoNEB algorithm executes the following procedure:

- The first step is to supplement any user-supplied images. If the number of user-supplied images is

less than N_{sim} , new images are added in the biggest geometrical gap as an image on the *image dependent pair potential* (IDPP) surface³⁴ or if requested as a linear interpolation of the atoms of the surrounding images.

- The main loop of the algorithm then proceeds with a normal NEB calculation focussing on the N_{sim} images centred on any newly added images until either of the convergence criteria specified below are reached.
- Then a new image is added either to increase the resolution in areas of rapid change in the potential energy surface or to improve the geometric resolution. The algorithm will put images in the biggest geometric gap if the inequality, defined in Eq. (4), is true. Otherwise, a new image will be added in a gap to strengthen the energy resolution,

$$\frac{f(\{\mathbf{R}_i\})}{g(\{E_i\})} > r_{se}, \quad (1)$$

$$f(\{\mathbf{R}_i\}) = \frac{\max(|\mathbf{R}_{i+1} - \mathbf{R}_i|)}{|\mathbf{R}_N - \mathbf{R}_1|}, \quad (2)$$

$$g(\{E_i\}) = \frac{\max(\Delta E_i)}{E_{\text{norm}}}. \quad (3)$$

With the energy difference, ΔE_i , the scaled energy difference, $\overline{\Delta E}_i$, and the average energy, $E_{\text{avg},i}$, between two images at image i , and the norm of the energy, E_{norm} , are defined as

$$\overline{\Delta E}_i = \Delta E_i h(E_{\text{avg},i}/E_{\text{norm}}), \quad (4)$$

$$h(x) = x, \quad (5)$$

$$E_{\text{norm}} = E_{\text{max}} - E_{\text{min}}, \quad (6)$$

$$E_{\text{avg},i} = \frac{E_{i+1} + E_i - 2E_{\text{min}}}{2}, \quad (7)$$

$$\Delta E_i = |E_{i+1} - E_i|. \quad (8)$$

The value of r_{se} is a user specified ratio between 0 and 1, which balances geometric and energy resolution

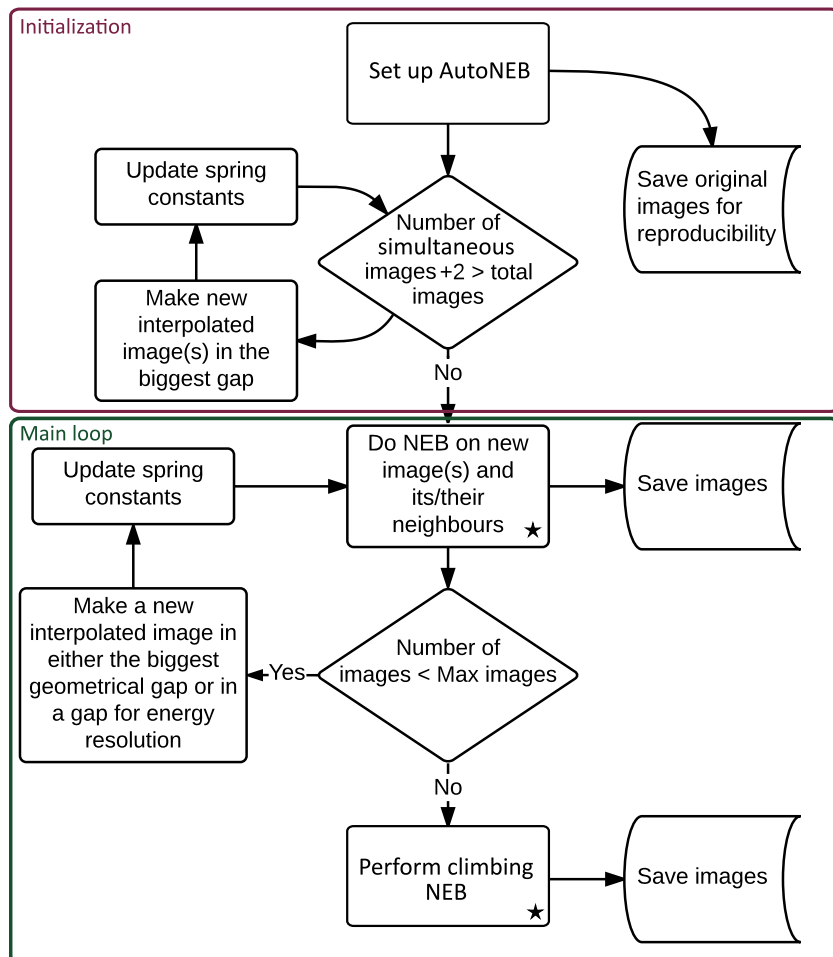


FIG. 2. The algorithm for the AutoNEB. In the two steps marked (\star), the NEB is stopped either if the forces have converged or if the maximum number of allowed force evaluations is reached.

considerations when searching for the MEP. $h(x)$ is a linear scaling introduced to favour new images inserted near the peak. When $r_{se} = 1$, a new image is always added in the gap of the biggest distance between two images. When $r_{se} = 0$, a new image is added solely to improve energy resolution between i and $i + 1$ where i is determined as the image where ΔE_i is the maximum. Figure 3 illustrates E_{norm} , $E_{avg,i}$, and ΔE_i used in Eq. (4) as well as the positions of image i and $i + 1$ on the reaction path as \mathbf{R}_i and \mathbf{R}_{i+1} .

By default, all images are added using the IDPP. The two new spring constants to the springs on either side of the new image are set so that they exactly replace the previous spring. This assures that adjacent images initially experience the same spring forces in the next iteration. In practice, the two new springs

will have double the spring constant of the replaced spring.

- The above two steps are repeated as an iterative process until the maximum number of images, N_{max} , is reached or, if specified, when a given resolution is obtained. Finally a climbing image NEB (CI-NEB)³⁵ is initialized with the highest energy image as the center of the NEB path.

The optional post-smoothing of the path that is outlined in the [supplementary material](#) can then be applied.

To converge an intermediate AutoNEB iteration either of the following two possible criteria should be met. The user specifies a maximum number of force evaluations per image per iteration after which the algorithm proceeds to the next step. If the maximum exerted force on any of the atoms is below a specified threshold before the maximum number of force evaluations is reached the algorithm is also considered converged and proceeds. For the last step where the TS is converged with the CI-NEB method (see below) only the maximum force exerted on any atom is relevant and as many force iterations as needed are used. To compare the effectiveness of the AutoNEB and the *all-image* NEB the total number of force evaluations is calculated by adding all relaxation steps for all images involved in creating the pathway. The

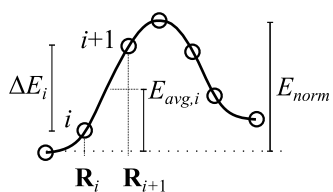


FIG. 3. A sketch of the assigned definitions of E_{norm} , $E_{avg,i}$, and ΔE_i .

resulting number is referred to as the “total number of force evaluations.”

B. Computational setup

ASE³³ was used to setup and optimize density functional theory (DFT) calculations as implemented in the GPAW³⁶ code as well for the calculations done with the Effective Medium Theory (EMT) potential.³⁷ In both computational setups, it is not important if parameters such as slab thickness, and for DFT the number of \mathbf{k} -points or basis set size, are converged, given that we are only interested in how effective the TS path finding methods are. For this reason, the selection of these parameters is based on speed and parallelizability.

DFT Method: For the DFT calculations the Perdew-Burke-Ernzerhof exchange-correlation functional³⁸ was chosen in combination with a simple linear combination of atomic orbitals with a double zeta polarized (dzp) basis for the wave functions.³⁹ Geometric optimizations were terminated when no force exerted on the atoms exceeded 0.025 eV/Å. For the AutoNEB, geometric optimizations were also terminated when the maximum number of force evaluations was reached progressing the algorithm to the next step. The calculations were performed in a stepped Pt(211) surface decorated with Ag. The chosen super cell spans two small terraces four atoms wide. This results in a two layer slab where periodic boundary conditions are applied in the direction parallel to the surface with at least 6 Å to the boundary of the cell perpendicular to the slab. The surface is shown in the top half of Figure 4. The bottom layer of the slab was held fixed to mimic the bulk material. To model an oxygen diffusion process on top of the surface an oxygen atom was adsorbed, cf., Figure 4. It is experimentally and theoretically shown that on the stepped Pt(211), surface oxygen prefers to chemisorb at the bridge sites of what would have been the Pt edge.^{40,41} The total number of atoms in each cell is 40, 8, and 1 of Pt, Ag, and O, respectively.

EMT Method: For the EMT potential,³⁷ a very similar surface cell was used and is displayed in the bottom half of Figure 4. The only difference is that one of the decorating Ag atoms has been exchanged with a Pt atom and that the atom diffusing on the surface is a Pt adatom. To calculate the adsorption potential energy (APE) for this Pt adatom as a function of the x and y coordinates, all but this Pt atom were constrained. A contour plot of the APE is displayed in the bottom of Figure 4 obtained by only relaxing the z coordinate of the Pt atom with 0.14 Å between grid points in the x - y -plane. EMT calculations were terminated when no force exerted on the atoms exceeded 0.025 eV/Å or if the maximum number of force evaluations was reached for the AutoNEB.

For the NEB implementation, a series of formulations are used and compared based on the total number of force evaluations used to converge to the TS, and to what degree the MEP follows the most direct pathway to and from a shared transition state. The regular NEB formulation²⁶ is used throughout the examples. For a number of examples, the regular NEB is further compared to what we consider a more robust method for finding transition states. This

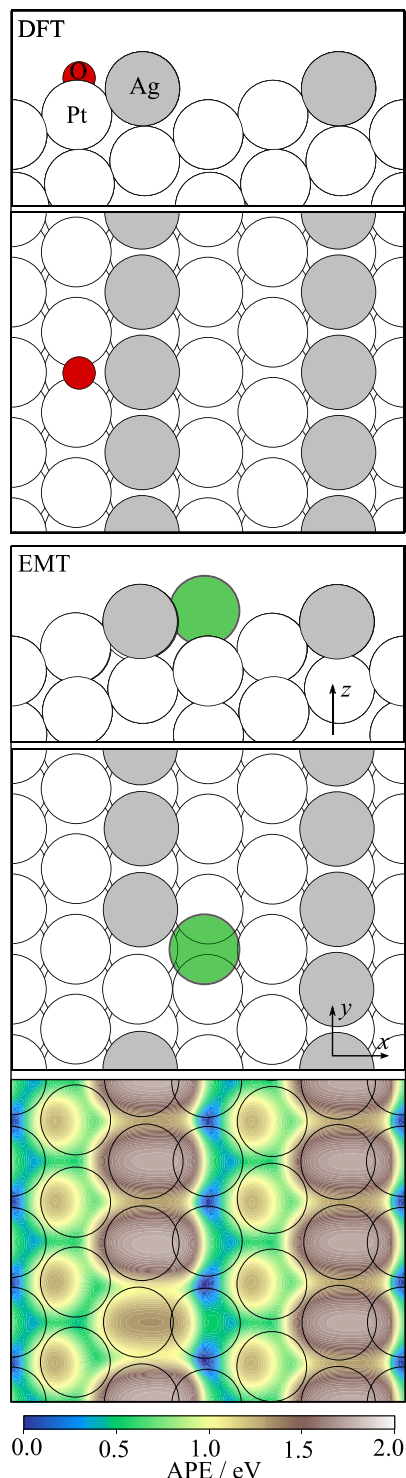


FIG. 4. The upper box displays the setup used for DFT calculations (O/Ag-stepped-Pt) while the bottom shows the setup for EMT calculations (Pt/Ag₃Pt/stepped-Pt) as well as the energy landscape for Pt adatom.

method relies on the combination of an elastic band (EB) and the climbing image method and will be referred to as CI-NEB.⁴² This EB uses, unlike the regular NEB, the distance between the initial and final images divided by the number of springs to determine the equilibrium distance of each spring. For the purpose of this paper, the EB approach is used exclusively together with a climbing image since the purpose is to locate TSs and a real elastic band without a

climbing image will cut corners²⁶ around the TS if the energy landscape is bending. The NEB and EB formulations used in the following examples can be found in Appendices B and C. The original NEB formulation, Appendix A, is also used for the following benchmarking example, but the results are left in the supplementary material Figure S2. CI-EB is one of a number of examples of adjustments that tries to improve upon the regular NEB method.^{31,43,44} In the case of locating the TS, the climbing image NEB (CI-NEB) method³⁵ was utilized no matter the NEB/EB formulation.

III. RESULTS AND DISCUSSION

A. Benchmarking

Benchmarking the AutoNEB against an *all-image* NEB scheme is done for a simple diffusion process following the setup described by the *DFT Method*. Moving an oxygen atom across the Ag row is associated with a barrier and locating the transition state fast and reliably is desirable. In Figure 5, the converged path is shown as well as the total number of force evaluations as a function of the NEB procedure used to complete the task. The two chosen NEB formulations, see Appendices B and C, are used for both the AutoNEB (shown here using a maximum of 35 force evaluations per intermediate AutoNEB iteration) and for an *all-image* NEB. For an extended picture, see the supplementary material Figure S2, where the total number of force evaluations is plotted as a function of the allowed intermediate force evaluations.

The calculations, supported by supplementary material Figure S2, clearly show that no matter the chosen NEB formulation the AutoNEB outperforms an *all-image* NEB when solving the task at hand, i.e., locating the TS for O diffusion over the Ag decorated Pt step. As also reported earlier, the method by which images are kept equally spaced, in this case the definition of the spring force, does not have a considerable impact on computational demand⁴⁵ as does switching from a regular NEB to an AutoNEB scheme.

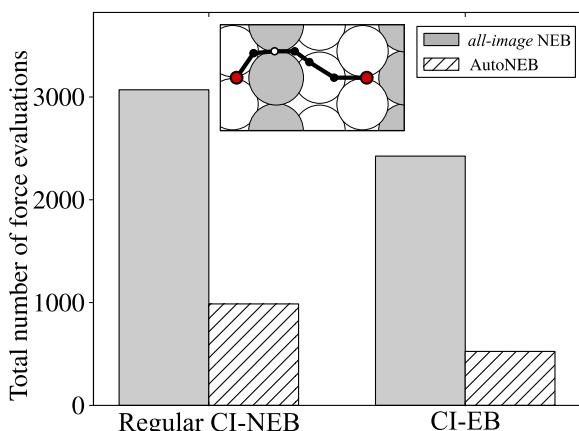


FIG. 5. Total number of force evaluations shown for an *all-image* NEB as the grey bars, while the hashed bars show the AutoNEB's performance using a maximum of 35 intermediate force evaluations.

We further tested the AutoNEB algorithm on a dehydrogenation reaction of pyridine on Pt(111) reported in the literature.⁶ Here the AutoNEB algorithm performs very well locating the TS in half as many force evaluations compared to the required force evaluations for the *all-image* NEB both utilizing a climbing image (6507 and 13 220 force evaluations, respectively). This demonstrates that the algorithm works well for a variety of tasks. In the supplementary material the precise calculations preformed can be found as well as an image of the converged pathways.

B. Pitfalls

In this section, we discuss two issues often encountered when performing NEB calculations—regardless of using the *all-image* or AutoNEB scheme. The first issue is that of assuring that not just some local pathway is found, but that the optimum pathway having the globally lowest possible energy at the critical TS is found. The other issue is concerned with the behavior of the regular NEB in a flat energy landscape or energy landscapes with many local minima. We point out and illustrate that the regular NEB method may result in pathways with long detours. As a solution to this we introduce the CI-EB method.

1. Dealing with multiple transition states

NEB is a method used to locate the TS/MEP in the vicinity of an initial path. However, for a given initial and final image, the optimum pathway may not lie along a direct path between these two images. In order to be certain that a calculated TS is along the optimum pathway, alternative pathways must be probed. An example of a linearly interpolated initial path (whether formed by an *all-image* NEB or by an AutoNEB) is displayed in the top left of Figure 6. It does not converge to the desired TS. As the problems become more complicated so do the corresponding multidimensional energy landscapes, which reduces the certainty of locating the correct result. This can, for instance, be seen in the case of pyridine and 2,2,2-trifluoroacetophenone (TFAP) diffusion on Pt(111).^{5,6} Taking the most direct path does not result in locating the correct TS and alternative pathways have to be considered. Different strategies can be utilized to explore other possible pathways between distant minima.^{46–48} In Figure 6, two methods are examined for Pt diffusion on a fully constrained Pt(211) surface with the edge partially decorated with Ag and Pt atoms as described by the *EMT Method* in Section II B. The underlying energy landscape is shown as a colored contour map, and the NEB paths, revealing the routes discovered by the two algorithms, are shown as red curves. The extensive search is of course redundant for this specific case, where we know the energy landscape, but the simplicity only stems from the very simple test system and mapping all of a multidimensional energy landscape is of course impractical if not impossible for more complex problems.

The first suggested option (“minima hopping”) is to locate all imaginable metastable configurations and interlinking the

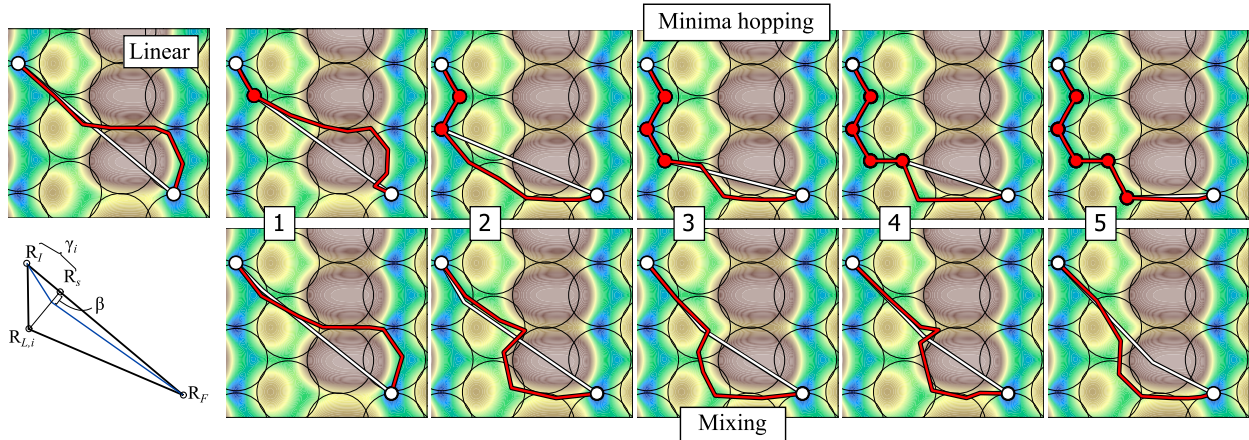


FIG. 6. The upper row shows the minima hopping strategy where neighboring minima (intermediate white and red circles) are connected in steps to complete the total path. The bottom row displays paths from mixing in minima in the neighborhood (same minima as for the minima hopping) and its progress towards the final reaction pathway.

neighboring minima and then proceed to calculate the barrier for each transition. The problem of finding the globally optimum path is then reduced to finding the route which takes you from the initial to the final image via local minima with the lowest critical TS as done in the upper panel of Figure 6.

Another option (“mixing”) is to mix neighboring minima in the initial linearly interpolated path thereby diverting the path from a direct route. The principle is shown in the lower panel of Figure 6 with the present example resulting in an initial path following the white line. For this option we propose an algorithm that locates a “support” point of the mixing by projecting a neighboring minimum, $\mathbf{R}_{L,i}$, on to the linear path between the initial and final state. The size of the projection,

$$\gamma_i = \frac{(\mathbf{R}_{L,i} - \mathbf{R}_I) \cdot (\mathbf{R}_F - \mathbf{R}_I)}{|\mathbf{R}_F - \mathbf{R}_I|^2},$$

then decides the “support” image,

$$\mathbf{R}_s = \mathbf{R}_I + \gamma_i(\mathbf{R}_F - \mathbf{R}_I),$$

position. The interpolation between the initial, \mathbf{R}_I , and final, \mathbf{R}_F , images with a mixing of a neighboring image, $\mathbf{R}_{L,i}$, then becomes

$$\mathbf{R}_i(\alpha) = \mathbf{R}_I + \alpha(\mathbf{R}_F - \mathbf{R}_I) + f(\alpha, \gamma_i)\beta(\mathbf{R}_{L,i} - \mathbf{R}_s), \quad (9)$$

with the switching function, $f(\alpha, \gamma_i)$, that depends on γ_i as

$$f(\alpha, \gamma_i) = \begin{cases} \frac{\alpha}{\gamma_i} & \text{for } \min(0, \gamma_i) \leq \alpha \leq \max(0, \gamma_i) \\ \frac{1-\alpha}{1-\gamma_i} & \text{for } \min(1, \gamma_i) \leq \alpha \leq \max(1, \gamma_i) \end{cases}.$$

In this work, the mixing parameter β was chosen to be 0.25. As a side note, in the limit of $\beta = 1$ the mixing scheme approaches the minima hopping.

In Figure 6, both methods solve the problem and locate the globally optimum TS while only in this particular case, the minima hopping transmit the Pt through the lowest possible energy region resulting in a pathway that gives more insight into a more realistic diffusion mechanism. The individual NEB paths have been evaluated with the AutoNEB

in combination with the regular NEB formulation found in Appendix B.

The minima hopping method was exploited for pyridine diffusion with great success.⁶ The mixing of neighboring minima was found beneficial in the search for the lowest barrier for TFAP diffusion⁵ in a slightly different implementation where γ was always set to 0.5.

2. Intrinsic instability of regular NEB

In the course of our work with the regular NEB method, we have often encountered that pathways deviate from the MEPs and that the overall path lengths may grow out of proportion. The problem is illustrated in Figures 7 and 8, where it is seen to persist even as the number of images is varied (Figure 7) or as spring constants are increased (Figure 8). The root cause for the instability can be traced to the formulation of the force-contribution from springs in the regular NEB formulation (see Appendix B for full details),

$$\mathbf{F}_i^s \|_\parallel = (|\mathbf{R}_{i+1} - \mathbf{R}_i|k_i - |\mathbf{R}_i - \mathbf{R}_{i-1}|k_{i-1})\hat{\tau}_i. \quad (10)$$

The magnitude of $\mathbf{F}_i^s \|_\parallel$ is seen to vanish whenever two adjacent springs are equally long, which is a necessary condition to distribute images evenly along the path. However, the expression is formulated so that $\mathbf{F}_i^s \|_\parallel$ vanishes irrespective of *how long* the springs are as long as they are of equal length. This allows the path to evolve into having very long segments that take the system on detours away from the direct MEP, visiting remote local minima. This can result in over-analyzing certain movements of the atoms allocating these as important steps in reaction mechanisms while just being an artifact of the relaxation process.

In the formulation of the regular NEB method,²⁶ the part of the spring force that is perpendicular to the local tangent is omitted. This is one of the cornerstones of the NEB since it assures that the spring forces do not drag the path up in the energy landscape where there is a bend in the curvature and hence eliminates the so-called *corner cutting* problem.²⁶ Using real springs instead is of course an issue if it results

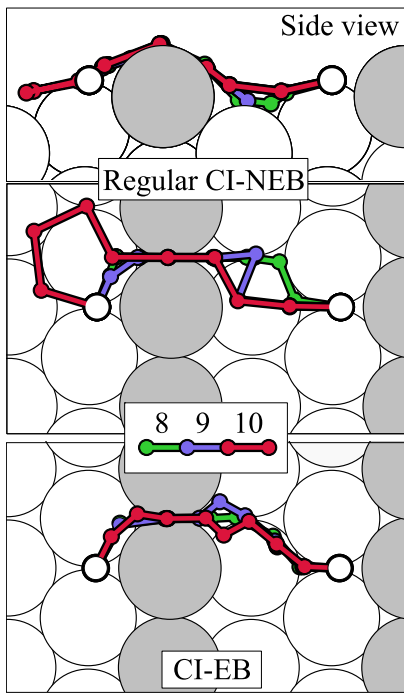


FIG. 7. Calculations with a spring force, $k = 1$, for the regular NEB formulation in the top two plots with the upper showing the side view and the middle image the top view for different number of images. At the bottom CI-EB is plotted for the same number of images as the regular NEB.

in corner cutting in the area of the energy landscape that is in the vicinity of the TS. This will result in an estimate of the barrier to be higher than what is actually true. However, the problem disappears if the TS is located with a CI-NEB, where the climbing image does not feel the spring forces. All that is required is a good guess for the two neighboring images to the CI-image that will then converge to the true

TS. However, the penalty is that the images along the path will not necessarily converge to the true MEP except for the climbing image when the full spring force is used (see also [supplementary material](#) Figure S3 where this is apparent). Another approach would be to return to the original NEB implementation, see [Appendix A](#), dealing with the possible kinks in the pathway by adding a switching function that penalizes kinks directly.^{48,49}

The difference between an elastic band as described in [Appendix C](#) and the regular NEB method in [Appendix B](#) where both are used with a climbing image NEB scheme is plotted in Figure 7. The problem is highlighted in the top half of Figure 7, which uses the regular NEB formulation to resolve the oxygen diffusion on the Pt(211) surface with the *DFT Method*.

Increasing the number of images and hence in theory improving the resolution of the MEP does not cure the problem; it only makes the issue worse. By using the CI-EB as in the bottom of Figure 7, the path converges towards a much more direct and reasonable path between the initial and final state without taking huge detours visiting other irrelevant minima, and moving the path away from the desired direction. Two videos showing how the two ten image NEBs converge are available in the [supplementary material](#).

The problem becomes even more evident if the initial guessed pathway lies very close to many local minima. In Figure 8 a case where an initial pathway (illustrated as a white line—most easily seen in the right hand plot) is constructed such that it includes many local minima. The initial path mimics what could have been a NEB in a complex energy landscape where many small less important local minima are located.

In Figure 8 the respective final paths (colored) are plotted depending on the NEB formulation and the choice of spring constant (calculated using the *EMT method*). The figure shows

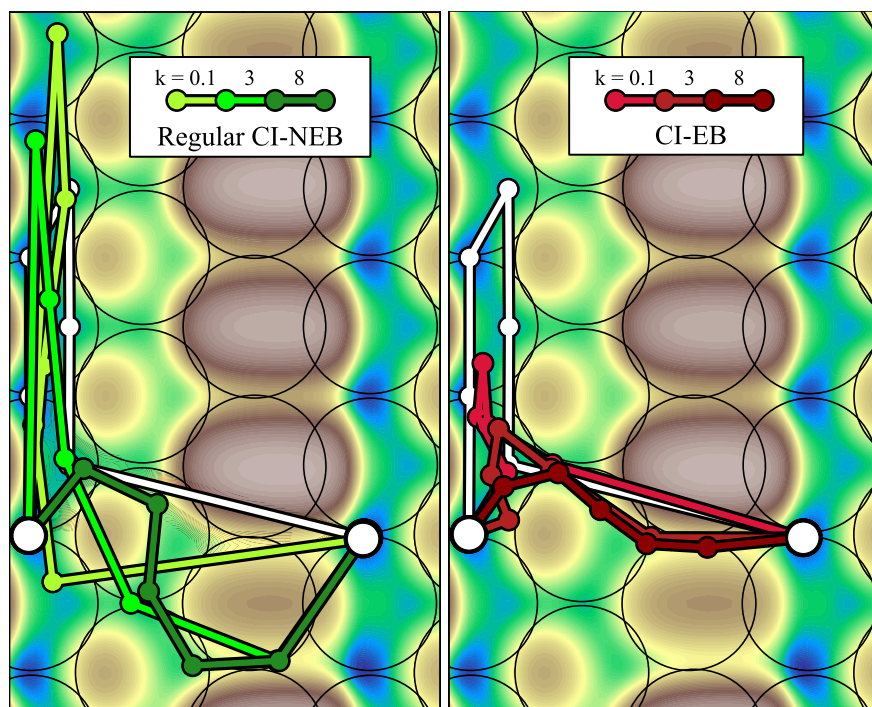


FIG. 8. For Pt diffusion on Ag decorated Pt(211) is the initial deliberately poorly “guessed” path plotted as white. To the left are shown three green relaxed paths for which a formulation of the spring force is given by the regular NEB while to the right three red curves using the CI-EB are depicted. The respective spring constants used to relax the paths are 0.1, 3, and 8 eV/Å².

that the individual images do not converge well to the MEP before both the spring force is high and CI-EB's real springs are introduced. The CI-EB method thus proves efficient in curing instability contained in the regular NEB as discussed in connection with Eq. (10). In Figure 8, the initial path was deliberately constructed so as to visit several local minima. Such a path seems unlikely to be chosen as an initial guess with the present problem, however working in a high-dimensional space one might inadvertently set up such an initial path based on knowledge of a number of local minima, and it is hence desirable that the method is robust enough to handle such a situation.

IV. CONCLUSIONS

The AutoNEB algorithm used to locate the barrier for oxygen diffusion on the Pt(211) surface decorated with Ag and for dehydrogenation of pyridine on a Pt(111) surface is shown to drastically reduce the number of steps needed to locate to the TS. It accomplishes this by first determining a rough outline of the MEP before increasing the resolution of the MEP at regions of highest interest to the user. In general, the lower number of force evaluations needed for the AutoNEB to locate the TS is especially pronounced for initial guessed paths that lie far away from the MEP. By introducing the autonomous AutoNEB, it becomes even more important to be aware of the different possible pitfalls when performing NEB calculations in order to recognise when results are anomalous. This includes exploring non-intuitive, alternative pathways with unique TSs. Here we have presented two successful methods to generate new images to include into the pathway: one that jumps between different minima and one of mixing in neighboring minima. If locating the TS is the objective, it is shown that resorting to an elastic band formulation, which includes a linear restoring force proportional to the distance between neighboring images, in combination with a climbing image appears to be a more robust and faster approach that yields a more direct pathway.

SUPPLEMENTARY MATERIAL

See the [supplementary material](#) for a smoothing extension to the AutoNEB algorithm and extensions to the benchmarking of the AutoNEB including two videos.

ACKNOWLEDGMENTS

We thank Hannes Jónsson for many fruitful discussions on the topic. Grants from the Danish Research Councils (Grant No. 0602-02566B) and The Lundbeck Foundation have supported this research.

APPENDIX A: ORIGINAL NEB

The original NEB formulation describes the local tangent as a bisection of the two neighboring normalized line segments,

$$\tau_i = \frac{\mathbf{R}_i - \mathbf{R}_{i-1}}{|\mathbf{R}_i - \mathbf{R}_{i-1}|} + \frac{\mathbf{R}_{i+1} - \mathbf{R}_i}{|\mathbf{R}_{i+1} - \mathbf{R}_i|} \quad (A1)$$

and from that the spring force parallel to the band together with the perpendicular true force is described as

$$\mathbf{F}_i^s|_{\parallel} = [(\mathbf{R}_{i+1} - \mathbf{R}_i)k_i - (\mathbf{R}_i - \mathbf{R}_{i-1})k_{i-1}] \cdot \hat{\tau}_i \hat{\tau}_i, \quad (A2)$$

$$\mathbf{F}_i = \mathbf{F}_i^s|_{\parallel} - \nabla V(\mathbf{R}_i)|_{\perp}, \quad (A3)$$

$$\nabla V(\mathbf{R}_i)|_{\perp} = \nabla V(\mathbf{R}_i) - \nabla V(\mathbf{R}_i) \cdot \hat{\tau}_i \hat{\tau}_i, \quad (A4)$$

where $\hat{\tau}_i = \tau_i / |\tau_i|$.

Initially, to deal with kinks appearing on the NEB path, a switching function not described here was introduced.²⁶

APPENDIX B: REGULAR NEB

With the departure of the original NEB formulation the switching function was a new, simpler NEB formulation.²⁶ Here the definition of the tangent follows the relative energies of the images as

$$\tau_i = \begin{cases} \tau_i^+ & \text{if } V_{i+1} > V_i > V_{i-1} \\ \tau_i^- & \text{if } V_{i+1} < V_i < V_{i-1} \\ \tau_i^+ \Delta V_i^{max} + \tau_i^- \Delta V_i^{min} & \text{if } V_{i+1} > V_{i-1} \\ \tau_i^+ \Delta V_i^{min} + \tau_i^- \Delta V_i^{max} & \text{if } V_{i+1} < V_{i-1} \end{cases}. \quad (B1)$$

The latter two only apply if i is at a minimum or a maximum. $\tau_i^+ = \mathbf{R}_{i+1} - \mathbf{R}_i$ and $\tau_i^- = \mathbf{R}_i - \mathbf{R}_{i-1}$ and

$$\Delta V_i^{max} = \max(|V_{i+1} - V_i|, |V_{i-1} - V_i|), \quad (B2)$$

$$\Delta V_i^{min} = \min(|V_{i+1} - V_i|, |V_{i-1} - V_i|). \quad (B3)$$

The spring force then becomes

$$\mathbf{F}_i^s|_{\parallel} = (|\mathbf{R}_{i+1} - \mathbf{R}_i|k_i - |\mathbf{R}_i - \mathbf{R}_{i-1}|k_{i-1}) \hat{\tau}_i, \quad (B4)$$

while the total force is calculated from the same expression as the original NEB,

$$\mathbf{F}_i = \mathbf{F}_i^s|_{\parallel} - \nabla V(\mathbf{R}_i)|_{\perp} \quad (B5)$$

$$\nabla V(\mathbf{R}_i)|_{\perp} = \nabla V(\mathbf{R}_i) - \nabla V(\mathbf{R}_i) \cdot \hat{\tau}_i \hat{\tau}_i, \quad (B6)$$

with $\hat{\tau}_i = \tau_i / |\tau_i|$.

APPENDIX C: ELASTIC BAND (EB)

While the kinks discussed in [Appendix A](#) might have diminished with the reformulation of the tangent and the spring force in the regular NEB ([Appendix B](#)) other problems can now occur due to the reduced complexity of the spring force. Another solution for well-behaved paths is the simple idea that builds on the use of real springs as in a plain elastic band method but borrows the nudging of the true force from the NEB method.²⁶ Here we describe the spring force as

$$\mathbf{F}_i^s|_{\parallel} = (|\tau_i^+| - L_{eq})k_i \frac{\tau_i^+}{|\tau_i^+|} - (|\tau_i^-| - L_{eq})k_{i-1} \frac{\tau_i^-}{|\tau_i^-|}, \quad (C1)$$

where N is the number of images,

$$L_{eq} = \frac{|\mathbf{R}_N - \mathbf{R}_1|}{N - 1}, \quad (C2)$$

$$\tau_i^- = \mathbf{R}_i - \mathbf{R}_{i-1}, \text{ and} \quad (C3)$$

$$\tau_i^+ = \mathbf{R}_{i+1} - \mathbf{R}_i. \quad (C4)$$

If i is a neighbor to i_{max} , it is non-static, and it is the climb NEB method whose formulation changes slightly,

$$\Delta V_i^{max} = \max(|V_{i+1} - V_i|, |V_{i-1} - V_i|), \quad (C5)$$

$$\Delta V_i^{min} = \min(|V_{i+1} - V_i|, |V_{i-1} - V_i|), \quad (C6)$$

$$\mathbf{F}_i^s|_{\parallel} = \left[(|\boldsymbol{\tau}_i^+| - L_{eq})k_i \frac{\boldsymbol{\tau}_i^+}{|\boldsymbol{\tau}_i^+|} - (|\boldsymbol{\tau}_i^-| - L_{eq})k_{i-1} \frac{\boldsymbol{\tau}_i^-}{|\boldsymbol{\tau}_i^-|} \right] \frac{\Delta V_i^{min}}{\Delta V_i^{max}}. \quad (C7)$$

Concerning the true force on the images it follows the idea from the original NEB method,

$$\boldsymbol{\tau}_i = \frac{\mathbf{R}_i - \mathbf{R}_{i-1}}{|\mathbf{R}_i - \mathbf{R}_{i-1}|} + \frac{\mathbf{R}_{i+1} - \mathbf{R}_i}{|\mathbf{R}_{i+1} - \mathbf{R}_i|}, \quad (C8)$$

$$\nabla V(\mathbf{R}_i)|_{\perp} = \nabla V(\mathbf{R}_i) - \nabla V(\mathbf{R}_i) \cdot \hat{\boldsymbol{\tau}}_i \hat{\boldsymbol{\tau}}_i, \quad (C9)$$

where $\hat{\boldsymbol{\tau}}_i = \boldsymbol{\tau}_i / |\boldsymbol{\tau}_i|$ and the total force is still given as

$$\mathbf{F}_i = \mathbf{F}_i^s|_{\parallel} - \nabla V(\mathbf{R}_i)|_{\perp}. \quad (C10)$$

- ¹J. Greeley and M. Mavrikakis, *Surf. Sci.* **540**, 215 (2003).
- ²O. R. Inderwildi, D. Lebiedz, O. Deutschmann, and J. Warnatz, *J. Chem. Phys.* **122**, 34710 (2005).
- ³N. Capron, P. Broqvist, and A. Pasquarello, *Appl. Phys. Lett.* **91**, 192905 (2007).
- ⁴H. Cheng and A. Selloni, *J. Chem. Phys.* **131**, 54703 (2009).
- ⁵G. Goubert, A. M. H. Rasmussen, Y. Dong, M. N. Groves, P. H. McBreen, and B. Hammer, *Surf. Sci.* **629**, 123 (2014).
- ⁶E. L. Kolsbjerg, M. N. Groves, and B. Hammer, *J. Chem. Phys.* **144**, 164112 (2016).
- ⁷D. Loffreda, D. Simon, and P. Sautet, *J. Chem. Phys.* **108**, 6447 (1998).
- ⁸M. R. Sørensen, Y. Mishin, and A. F. Voter, *Phys. Rev. B* **62**, 3658 (2000).
- ⁹I. M. Ciobăcă, F. Frechard, R. A. Van Santen, A. W. Kleyn, and J. Hafner, *J. Phys. Chem. B* **104**, 3364 (2000).
- ¹⁰K. Honkala and K. Laasonen, *Phys. Rev. Lett.* **84**, 705 (2000).
- ¹¹M.-L. Bocquet, A. Michaelides, D. Loffreda, P. Sautet, A. Alavi, and D. A. King, *J. Am. Chem. Soc.* **125**, 5620 (2003).
- ¹²E. Jiang and E. A. Carter, *Surf. Sci.* **570**, 167 (2004).
- ¹³J. Greeley and M. Mavrikakis, *Nat. Mater.* **3**, 810 (2004).
- ¹⁴S. Sakong and A. Groß, *J. Catal.* **231**, 420 (2005).
- ¹⁵D. Loffreda, F. Delbecq, F. Vigné, and P. Sautet, *J. Am. Chem. Soc.* **128**, 1316 (2006).
- ¹⁶C. Dupont, Y. Jugnet, and D. Loffreda, *J. Am. Chem. Soc.* **128**, 9129 (2006).
- ¹⁷H. Fu, Z.-P. Liu, Z.-H. Li, W.-N. Wang, and K.-N. Fan, *J. Am. Chem. Soc.* **128**, 11114 (2006).
- ¹⁸D. Torres, N. Lopez, F. Illas, and R. M. Lambert, *Angew. Chem., Int. Ed.* **46**, 2055 (2007).
- ¹⁹D. Borthwick, V. Fiorin, S. J. Jenkins, and D. A. King, *Surf. Sci.* **602**, 2325 (2008).
- ²⁰O. R. Inderwildi and S. J. Jenkins, *Chem. Soc. Rev.* **37**, 2274 (2008).
- ²¹O. R. Inderwildi, S. J. Jenkins, and D. A. King, *J. Phys. Chem. C* **112**, 1305 (2008).
- ²²Y. Pan, C. Liu, and Q. Ge, *J. Catal.* **272**, 227 (2010).
- ²³R. B. Getman and W. F. Schneider, *ChemCatChem* **2**, 1450 (2010).
- ²⁴F. Auneau, L. S. Arani, M. Besson, L. Djakovitch, C. Michel, F. Delbecq, P. Sautet, and C. Pinel, *Top. Catal.* **55**, 474 (2012).
- ²⁵B. T. Loveless, C. Buda, M. Neurock, and E. Iglesia, *J. Am. Chem. Soc.* **135**, 6107 (2013).
- ²⁶G. Henkelman and H. Jónsson, *J. Chem. Phys.* **113**, 9978 (2000).
- ²⁷L. J. Munro and D. J. Wales, *Phys. Rev. B* **59**, 3969 (1999).
- ²⁸R. Malek and N. Mousseau, *Phys. Rev. E* **62**, 7723 (2000).
- ²⁹G. Henkelman and H. Jónsson, *J. Chem. Phys.* **111**, 7010 (1999).
- ³⁰J.-W. Chu, B. L. Trout, and B. R. Brooks, *J. Chem. Phys.* **119**, 12708 (2003).
- ³¹S. A. Trygubenko and D. J. Wales, *J. Chem. Phys.* **120**, 2082 (2004).
- ³²L. Xie, H. Liu, and W. Yang, *J. Chem. Phys.* **120**, 8039 (2004).
- ³³S. R. Bahn and K. W. Jacobsen, *Comput. Sci. Eng.* **4**, 56 (2002).
- ³⁴S. Smidstrup, A. Pedersen, K. Stokbro, and H. Jónsson, *J. Chem. Phys.* **140**, 214106 (2014).
- ³⁵G. Henkelman, B. P. Uberuaga, and H. Jónsson, *J. Chem. Phys.* **113**, 9901 (2000).
- ³⁶J. Enkovaara, C. Rostgaard, J. J. Mortensen, J. Chen, M. Duak, L. Ferrighi, J. Gavnholm, C. Glinsvad, V. Haikola, H. A. Hansen, H. H. Kristoffersen, M. Kuisma, A. H. Larsen, L. Lehtovaara, M. Ljungberg, O. Lopez-Acevedo, P. G. Moses, J. Ojanen, T. Olsen, V. Petzold, N. A. Romero, J. Stausholm-Møller, M. Strange, G. A. Tritsaris, M. Vanin, M. Walter, B. Hammer, H. Häkkinen, G. K. H. Madsen, R. M. Nieminen, J. K. Nørskov, M. Puska, T. T. Rantala, J. Schiøtz, K. S. Thygesen, and K. W. Jacobsen, *J. Phys.: Condens. Matter* **22**, 253202 (2010).
- ³⁷K. W. Jacobsen, P. Stoltze, and J. K. Nørskov, *Surf. Sci.* **366**, 394 (1996).
- ³⁸J. P. Perdew, K. Burke, and M. Ernzerhof, *Phys. Rev. Lett.* **77**, 3865 (1996).
- ³⁹A. H. Larsen, M. Vanin, J. J. Mortensen, K. S. Thygesen, and K. W. Jacobsen, *Phys. Rev. B* **80**, 195112 (2009).
- ⁴⁰P. Gambardella, Ž. Šljivančanin, B. Hammer, M. Blanc, K. Kuhnke, and K. Kern, *Phys. Rev. Lett.* **87**, 056103 (2001).
- ⁴¹Ž. Šljivančanin and B. Hammer, *Surf. Sci.* **515**, 235 (2002).
- ⁴²H. Jónsson, private communication (2016).
- ⁴³P. Maragakis, S. A. Andreev, Y. Brumer, D. R. Reichman, and E. Kaxiras, *J. Chem. Phys.* **117**, 4651 (2002).
- ⁴⁴M. Melander, K. Laasonen, and H. Jónsson, *J. Chem. Theory Comput.* **11**, 1055 (2015).
- ⁴⁵D. Sheppard, R. Terrell, and G. Henkelman, *J. Chem. Phys.* **128**, 134106 (2008).
- ⁴⁶D. J. Wales, *Mol. Phys.* **100**, 3285 (2002).
- ⁴⁷J. M. Carr, S. A. Trygubenko, and D. J. Wales, *J. Chem. Phys.* **122**, 234903 (2005).
- ⁴⁸E. Maras, O. Trushin, A. Stukowski, T. Ala-Nissila, and H. Jónsson, *Comput. Phys. Commun.* **205**, 13 (2016).
- ⁴⁹H. Jónsson, G. Mills, and K. W. Jacobsen, “Nudged elastic band method for finding minimum energy paths of transitions,” in *Classical and Quantum Dynamics in Condensed Phase Simulations*, edited by B. J. Berne, G. Ciccotti and D. F. Coker, **385** (World Scientific, 1998).